Observation of localized multi-spatial-mode quadrature squeezing

C. S. Embrey,[1] M. T. Turnbull,[1,2] P. G. Petrov,[1] and V. Boyer[1]

[1] *Midland Ultracold Atom Research Centre, School of Physics and Astronomy, University of Birmingham, Edgbaston, Birmingham B15 2TT, UK*

[2] *Gravitational Research Group, Physics Department, John Anderson Building, University of Strathclyde, Glasgow, G4 0NG, UK*

(Dated: June 10, 2015)

Quantum states of light can improve imaging whenever the image quality and resolution are limited by the quantum noise of the illumination. In the case of a bright illumination, quantum enhancement is obtained for a light field composed of many squeezed transverse modes. A possible realization of such a multi-spatial-mode squeezed state is a field which contains a transverse plane in which the local electric field displays reduced quantum fluctuations at all locations, on any one quadrature. Using a travelling-wave amplifier, we have generated a multi-spatial-mode squeezed state and showed that it exhibits localised quadrature squeezing at any point of its transverse profile, in regions much smaller than its size. We observe 75 independently squeezed regions. The amplification relies on nondegenerate four-wave mixing in a hot vapor and produces a bichromatic squeezed state. The result confirms the potential of this technique for producing illumination suitable for practical quantum imaging.

arXiv:1409.6561v2 [quant-ph] 8 Jun 2015

I. INTRODUCTION

When performed with a classical light source, optical measurements are limited by the quantum fluctuations of the electromagnetic field, which produce noise at the so-called quantum-noise level (QNL). It is however possible to improve on the QNL using quantum states of light, for instance squeezed light [1]. To be useful for full-field-of-view imaging applications, a quantum state of light must be spatially multimode, so that it can probe or carry spatial information [2]. Recently there has been substantial progress in few-photon quantum imaging techniques, where the illumination is very low and the photons are detected individually. These few-photon entangled states have yielded clearer images than those produced by the equivalent classical illuminations, whose QNL-limited signal-to-noise ratios are nominally poor. In particular, these states have produced images of amplitude [3] and phase [4, 5] objects with noise below the QNL, and interferences displaying better spatial resolution [6]. These experiments do not rely on the ability of generating a high level of quadrature squeezing, which remains usually very low, but rather on the possibility of generating few photon pairs with a good fidelity using low-gain parametric downconversion in a nonlinear crystal.

Although very low-level illumination may be required in select applications, there is a broader interest in applying quantum imaging techniques to the cases were a bright illumination can be applied. In this case, the signal-to-noise ratio at the QNL is much higher and quantum light, specifically quadrature-squeezed light, can provide an improvement over an already optimised classical detection. Unlike for the few-photon illumination, quantum noise reduction with bright illumination is achieved using strong quadrature squeezing.

The benefit of squeezed light to determine the position of a fixed particle has already been demonstrated in a biological environment with a single squeezed mode [7]. Quantum enhanced imaging of a more complex object can also be achieved by squeezing the relevant mode in optical scanning microscopy techniques [8]. However, improving the spatial resolution in a single-shot imaging of the full field of view would require a multi-spatial-mode (MSM) quadrature-squeezed light field [9]. Whilst efficient multimode generation of squeezed light has been reported in optical parametric oscillators in the time domain [10, 11], the realisation of quadrature squeezing in a large number of spatial modes has remained a long-standing goal in the field of quantum optics [12]. The main hurdle in the generation of MSM-squeezed light has been the lack of an available strong multimode nonlinearity. Enhancing weak nonlinearities in $\chi^{(2)}$ crystals with a spatially degenerate cavity is feasible [13], and in principle scalable, but success has been limited to a small number of spatial modes [14]. A possible solution is to operate without a cavity in a pulsed regime, where large peak pump intensities lead to large levels of squeezing. However this approach has been limited to producing correlations between twin beams (two-mode squeezed state) [15–17] rather than producing a single squeezed beam. Another workaround is the direct engineering of overlapping squeezed modes [18] but practical scalability is also lacking.

An alternative to parametric downconversion are the large resonant $\chi^{(3)}$ atomic nonlinearities that have been shown to be promising alternatives for the production of quantum field correlations in the spatial domain [19, 20]. In this paper, we report on using such nondegenerate four-wave mixing (4WM) in a hot vapor as a large-gain multimode amplifier. This has allowed us to generate a vacuum which is quadrature-squeezed in a large number of spatial modes. In particular we have demonstrated localised vacuum quadrature squeezing, in a configuration which, when superimposed to a bright coherent state, would be suitable for enhanced optical resolution appli-

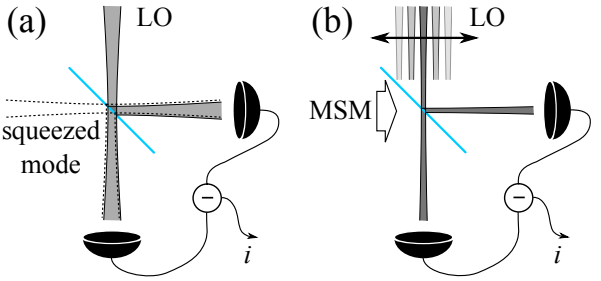

Figure 1. The homodyne detection of a squeezed state leads to reduced noise on the balanced photo-current i below the QNL. (a) For a single spatial mode squeezed state the mode of the LO must match the squeezed mode. (b) For a hypothetical multi-spatial-mode squeezed state (MSM) the LO could have any shape or position.

cations.

II. BACKGROUND

In free space, an optical mode is described quantum-mechanically by the field quadrature operators X and Y. The noncommutativity of X and Y implies a Heisenberg inequality $\Delta X \Delta Y \geq \frac{1}{4}$ which is responsible for the quantum fluctuations of the electromagnetic field. The QNL is reached when the inequality is saturated—it then describes a so-called minimum uncertainty state—and the uncertainties on both quadratures are equal. It is possible to reduce, or "squeeze", the uncertainty on one of the quadratures below the QNL, as long as it is compensated by an equal increase on the other quadrature.

To illustrate the key signature of a MSM-squeezed state let us first consider the homodyne detection of a single-mode squeezed state. In such a configuration, a bright local oscillator (LO) beats with the squeezed mode and amplifies the fluctuations of one of its quadratures [Fig. 1(a)]. Because the LO selects the spatial mode to be analysed, it is important to achieve a good overlap between the optical modes of the LO and the squeezed field. Soon after the first observation of squeezed light [21] , the question of "local" squeezing was raised [12], that is to say the possibility of generating and observing a light field with reduced quantum fluctuations at any point of its transverse profile. Equivalently, such a field would display quadrature squeezing on a homodyne detector operated with an arbitrary spatial configuration of the LO [22], as depicted in Fig. 1(b). This MSM-quadrature-squeezed field has been theoretically shown to allow an improvement of the spatial resolution beyond the QNL in certain schemes of optical super-resolution [9], but its efficient generation has remained elusive until the present work.

To describe more formally the properties of a MSM-squeezed state, let us consider a light field propagating along the z axis, in a minimum uncertainty state, such that in the near field ($z = 0$) the Y quadrature is squeezed at all points $\boldsymbol{\rho}$ in the transverse plane: $\Delta Y(\boldsymbol{\rho}) < \frac{1}{2}$. Classically, and in the Fraunhofer diffraction limit, the transverse distribution of the far electric field at $z = \infty$ is the Fourier transform $E(\mathbf{q})$ of the transverse distribution $E(\boldsymbol{\rho})$ of the near electric field. Quantum mechanically, this property results in quantum correlations in the far field between positions $\mathbf{q}$ and $-\mathbf{q}$ due to the joint quadratures $X_-(\mathbf{q}) = [X(\mathbf{q}) - X(-\mathbf{q})]/\sqrt{2}$ and $Y_+(\mathbf{q}) = [Y(\mathbf{q}) + Y(-\mathbf{q})]/\sqrt{2}$ being squeezed for all $\mathbf{q}$ (Appendix A).

Such a state can be created by a travelling-wave amplifier. This device creates Stokes and anti-Stokes fields (called twin beams, or probe and conjugate, or signal and idler) at the sideband frequencies $-\Omega$ and Ω with respect to a central frequency ω_0, which classically fulfil the phase conjugation $E(-\Omega) = E^*(\Omega)$ [23]. For a thin amplifier diffraction during the propagation is negligible and the phase conjugation at the output retains its local character: $E(\boldsymbol{\rho}, -\Omega) = E^*(\boldsymbol{\rho}, \Omega)$ for all $\boldsymbol{\rho}$. Quantum mechanically, this local phase conjugation translates into local quantum correlations in the near field (i.e. at the position where they are created in the amplifier). Specifically the quantum fluctuations of the joint quadratures $X_-(\boldsymbol{\rho}, \Omega) = [X(\boldsymbol{\rho}, \Omega) - X(-\boldsymbol{\rho}, \Omega)]/\sqrt{2}$ and $Y_+(\boldsymbol{\rho}, \Omega) = [Y(\boldsymbol{\rho}, \Omega) + Y(\boldsymbol{\rho}, -\Omega)]/\sqrt{2}$ are reduced below the QNL, while the similarly defined joint quadratures $X_+(\boldsymbol{\rho}, \Omega)$ and $Y_-(\boldsymbol{\rho}, \Omega)$ are anti-squeezed. When the probe and conjugate fields are degenerate, i.e. when $\Omega = 0$, this naturally leads the Y quadrature to be squeezed at dc in the near field.

The amount of squeezing is directly related to the thin amplifier gain If the gain is too low, a resonant cavity can be used provided it is spatially degenerate [13]. Experimentally this proves challenging [14] and a large gain travelling-wave amplifier may be preferable, for instance a 4WM process in a hot atomic vapour [24].

This nonlinear atomic system has been used to demonstrate symmetric correlations in the far field; in a non-degenerate configuration it gives rise to entangled images [25] while in a degenerate configuration it produces quadrature squeezing for centrally symmetric modes [20]. The local multimode operation of the device was also evidenced by noiseless amplification of near-field images [26]. Here we report on the direct measurement of the local squeezing of a MSM-squeezed state using a homodyne detector with an arbitrarily shaped LO, as shown in Fig. 1(b).

III. FOUR WAVE MIXING AS A TRAVELLING WAVE AMPLIFIER

We use the $D1$ line of rubidium 85 to generate probe and conjugate fields, using the 4WM scheme shown in Fig. 2 [24]. A single pump beam, at frequency ω_0, couples a probe field, at frequency $\omega_p = \omega_0 - \Omega$, with a conjugate field, at frequency $\omega_c = \omega_0 + \Omega$, where Ω is of the order

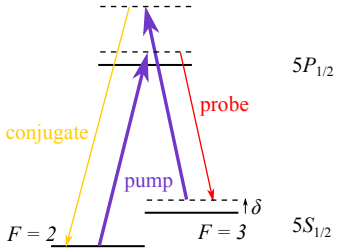

Figure 2. Nondegenerate four-wave-mixing scheme on the $D1$ line of ^{85}Rb. A single pump field creates correlations between the probe and conjugate fields, whose frequencies are separated by roughly twice the ground-state hyperfine splitting.

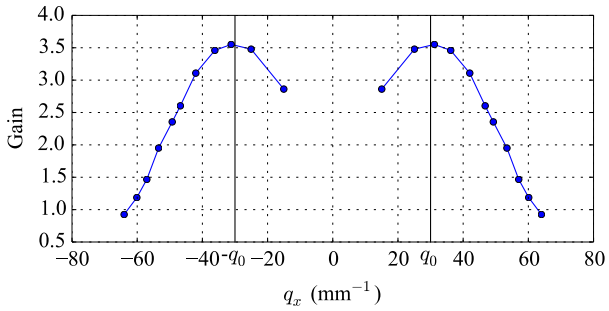

Figure 3. Spatial gain spectrum as inferred from the spatial gain profile in the far field. The probe field is seeded with a Gaussian beam at a variable angle with the pump beam and the ratio between the seed power and output probe power is measured. The profile has been measured along the x direction, but would be the same along any radial direction. The gain at low q_x is not accurately measurable due to pump light leakage at $q_x = 0$.

of the ground-state hyperfine splitting (≈ 3 GHz). The process is efficient for a range of detunings δ between the pump-probe Raman transition and the hyperfine splitting. This effectively sets the squeezing bandwidth $\Delta\Omega$ to ≈ 20 MHz.

The phase-matching condition, which requires the probe and conjugate fields to propagate symmetrically on opposite sides of the pump, is relaxed by the finite length of the rubidium cell. As a result a large number of pairs of modes, propagating along slightly different directions, are coupled by the 4WM process [19, 27]. Although the 4WM follows a co-propagating configuration (forward 4WM), dispersion of the index of refraction induces a small angle between the pump axis and the direction of maximum probe gain [28]. The resulting far- field spatial gain profile (Fig. 3) shows that the spatial gain spectrum peaks for a finite value of $|\mathbf{q}|$ and is reduced close to $|\mathbf{q}| = 0$. Consequently the region of substantial gain forms an annulus due to the axial symmetry around the z axis (Fig. 4). The gap in the gain around $|\mathbf{q}| = 0$ means that probe and conjugate modes with low transverse spatial frequencies are only weakly coupled by the 4WM process and cannot develop strong quantum correlations. To fix this shortcoming, we can use modes whose probe and conjugate spatial frequency spectra are each confined to opposite restricted gain regions (RGRs) of the gain annulus. These confined modes see a gapless effective gain spectrum in both the x and y directions for both their probe and conjugate components (Fig. 4).

In order to avoid the separate propagation of these restricted probe and conjugate modes, imposed by the phase-matching condition, we overlap on a beam-splitter two correlated propagation axes (A_1 and A_2) corresponding to positions $\pm\mathbf{q}_0$ in the far field. The direction of $\mathbf{q}_0$ is arbitrarily chosen to be along the x radial direction, as shown in Fig. 4. For the matched RGRs to overlap properly the magnitude q_0 must lie close to the middle point of the effective gain spectrum (Fig. 3). Redefining the overlapped A_1 and A_2 axes as the main optical axis the resulting output field is

$$E'(\mathbf{q},\Omega) = \frac{1}{\sqrt{2}}[E(\mathbf{q}+\mathbf{q}_0,\Omega) + E(\mathbf{q}-\mathbf{q}_0,\Omega)], \quad (1)$$

where the x coordinate of the redefined $\mathbf{q}$ is restricted to the region $[-q_0, q_0]$. It can be shown (Appendix A) that the output field exhibits far-field correlations that are symmetric with respect to $\mathbf{q}_0$, that is to say with respect to the new optical axis, and that the near-field spatial squeezing spectrum is derived from the gapless effective spectrum. It therefore contains all the spatial frequencies centred on dc and in a bandwidth of the order of q_0.

At this stage we have engineered a field with local correlations in the near field, which spans a bandwidth $\Delta\Omega = 30$ MHz and connects frequency sidebands separated by twice the hyperfine splitting, $2\Omega \approx 6$ GHz. This composite field forms our squeezed signal. A homodyne detector using a single-frequency LO at ω_0 would reveal the squeezing around an analysing frequency of ≈ 3 GHz. Instead we use a bichromatic local oscillator (BLO) as proposed by Marino et al. [29], where the single frequency component is replaced by two frequency components, one for each of the probe and conjugate sidebands.

Since each frequency component is resonant with one of the correlated sidebands, the BLO translates the squeezing spectrum from ≈ 3 GHz down to dc and the resulting noise on the photo-current i has the similar form to that of quadrature squeezing measured by a monochromatic LO [29]:

$$\langle \Delta i^2 \rangle \propto e^{2s}\cos^2\left(\frac{\chi_p + \chi_c - \theta_s}{2}\right) + e^{-2s}\sin^2\left(\frac{\chi_p + \chi_c - \theta_s}{2}\right), \quad (2)$$

where $\chi_{p,c}$ represents the phase difference between the LO and the signal for the probe and conjugate components respectively; θ_s is the squeezing angle; s is the squeezing parameter.

We use a separate 4WM process to generate the required frequency components of the BLO. A seed field at the probe frequency in one RGR stimulates the generation of bright amplified probe and conjugate fields in

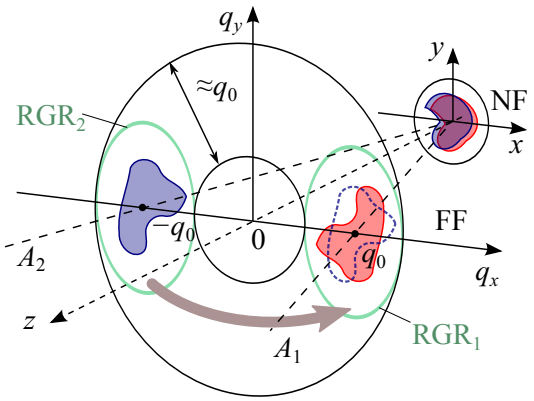

Figure 4. Geometry of the localised squeezing preparation. A 4WM gain medium in the near field (NF) produces local quantum correlations between the Ω and the $-\Omega$ sidebands. As a result, overlapped modes fulfilling the phase conjugation relation are correlated (twin mode 1 and twin mode 2, represented as overlapped colored regions in the near field). After propagation to the far field (FF) those correlated modes are contained in a annulus-shaped region resulting from the phase matching condition. On this diagram, we only represent the positive-q_x part of twin mode 1 and the correlated negative-q_x part of twin mode 2. These correlated modes follow the z-axial symmetry imposed by the phase-matching condition and we further assumed that they are contained in restricted gain regions (RGR) that are on the q_x axis. In order to create a multi-spatial-mode squeezed field which is fully included in a RGR, i.e. in a simply-connected gain region in the far field, one can superpose RGR$_2$ on RGR$_1$ on a 50/50 beamsplitter (not shown on this diagram) and select A_1 as the new optical axis. This is equivalent to translating the spectrum of the field in RGR$_2$ by q_0 and the spectrum of the field in RGR$_1$ by $-q_0$ along q_x.

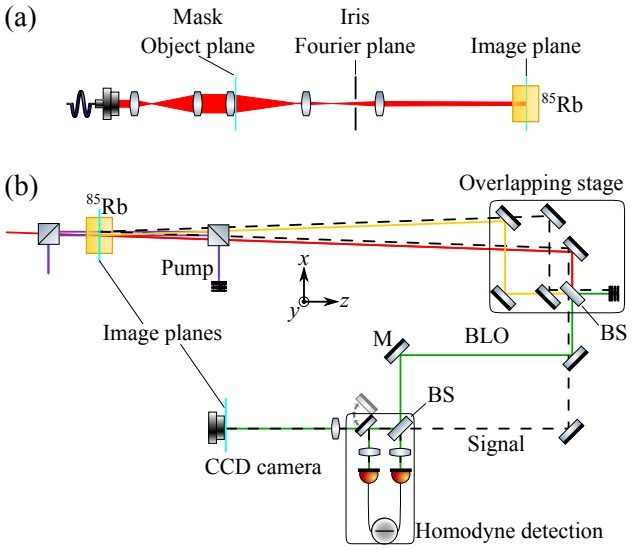

Figure 5. Schematic diagram of the setup. (a) shows the path of the seed to the vapor cell, with mask and filtering iris positions. (b) shows the creation and measurement of the squeezed vacuum. The black dashed lines depict the vacuum fields, which at all points contain both the probe and conjugate frequencies. The solid lines depict bright fields. The red and yellow represent probe and conjugate LO frequencies respectively. The green represents the BLO, and the purple the pump field. The cyan lines show the mask object and images positions. Where the vacuum and LO fields are slightly offset in the diagram they are actually separated vertically in the experiment. Nonetheless we use a single beamsplitter for both of them in the overlapping stage.

opposite RGRs. These are superimposed on the overlapping beamsplitter to form the BLO (Fig. 5), in a similar manner as for the squeezed signal field. This produces a bright bichromatic beam whose two frequency components tend to propagate along the same axis and have the same mode shape in the near field. We will see in section V B that this field has the right properties for the BLO.

IV. EXPERIMENTAL SETUP

A simplified experimental setup is shown in Fig. 5. A single heated rubidium cell is pumped by a pair of parallel pump beams, thus producing two non-overlapping 4WM amplifiers. A set of mirrors and a beamsplitter overlap a pair of matched RGRs as in Fig. 4. This operation is realised for both 4WM amplifiers. To generate the BLO we seed one of the amplifiers, at the probe frequency, with a mode that is contained within one of the RGRs. The other amplifier is left unseeded to generate the signal field. The resulting BLO and signal fields are fed into a homodyne detector to measure the noise on the signal.

The relative phase between the signal and LO fields, which controls the measured signal quadrature, is tuned by adjusting the optical path length of the BLO with a piezo-electric actuator. Using this method we have generated squeezing levels of up to 3.6 dB as show in Fig. 6.

Since our main experimental aim is to investigate the local character of the quantum correlations, we need to shape the BLO in the near field identically for both frequency components. This is achieved by shaping the seed with a mask which is optically conjugated with the gain medium [Fig. 5(a)]. High spatial frequencies, introduced by the mask, are filtered out with an aperture located in the Fourier plane. In the same way, the position of the BLO in the near field is controlled by steering the seed beam before the cell. The actual mode shape and position of the BLO can be recorded with an imaging lens located after the overlapping beamsplitter. More experimental details can be found in Appendix B.

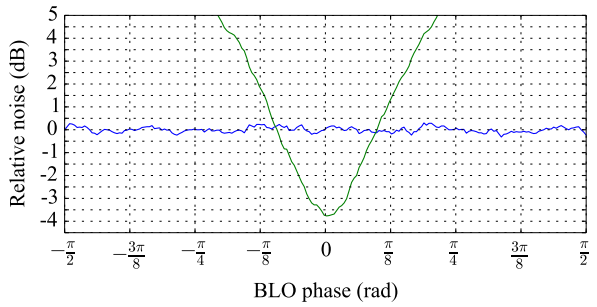

Figure 6. Typical squeezing graph, generated by scanning the phase difference between BLO and signal fields. For this data the LO pump power is 900 mW, the signal pump power is 950 mW and the gain is around 4. The electronic noise floor can also be subtracted, revealing a squeezing level of 3.8 dB.

V. RESULTS

A. Multimode squeezing

At this stage we have a MSM–quadrature-squeezed field, which should presents local quadrature squeezing, and a LO capable of analysing it. The steps described above to produce this field are required to remedy issues specific to our 4WM process, namely the existence of gaps in the spatial and frequency spectra of the gain. Beyond this apparent complexity, the local squeezing is the usual consequence of the creation of local correlations inside the amplifying medium. The signal field and BLO can be used to realise the simple experiment described in Fig. 1, that is to say they can display squeezing in a homodyne detector arrangement for an arbitrary transverse position of the BLO.

We want to show the local character of the squeezing on two perpendicular directions, completing the measurement on one direction at a time. To this effect we reduce the size of the BLO mode along the direction of interest, using a slit as the mask, while allowing the BLO mode to retain its full extent in the perpendicular direction.

The near-field BLO mode shape and the signal quadrature squeezing are recorded as the BLO is moved across the near field in the direction of its narrow size, whilst keeping its direction of propagation constant. A Gaussian fit of the BLO profile gives both its size, which remains constant, and position. Figure 7 shows the degree of squeezing as a function of the position of the BLO. The green squares and panels (b) and (e) show the squeezing using a gain of around 4. They clearly demonstrate local squeezing over a wide range of non-overlapping positions of the BLO in both directions and thus the highly-MSM nature of the system.

So far we have assumed a thin medium at $z = 0$, in practice the cell has a finite length of 12.5 mm, and propagation effects cannot be fully neglected. A mode of very small transverse size will inevitability diffract over the length of the gain medium and as a result the correlations cannot be fully local. This gives rise to a minimum area over which local squeezing can be observed, referred to as the coherence area, and a corresponding coherence length [30]. In the above results we have used a BLO with its smaller dimension chosen such that a reasonable level of squeezing remains. In the blue circles and panels (c) and (f) in Fig. 7 the gain is reduced to around 2 and squeezing can be observed for a smaller slit width, and over a larger range of positions, albeit at a lower

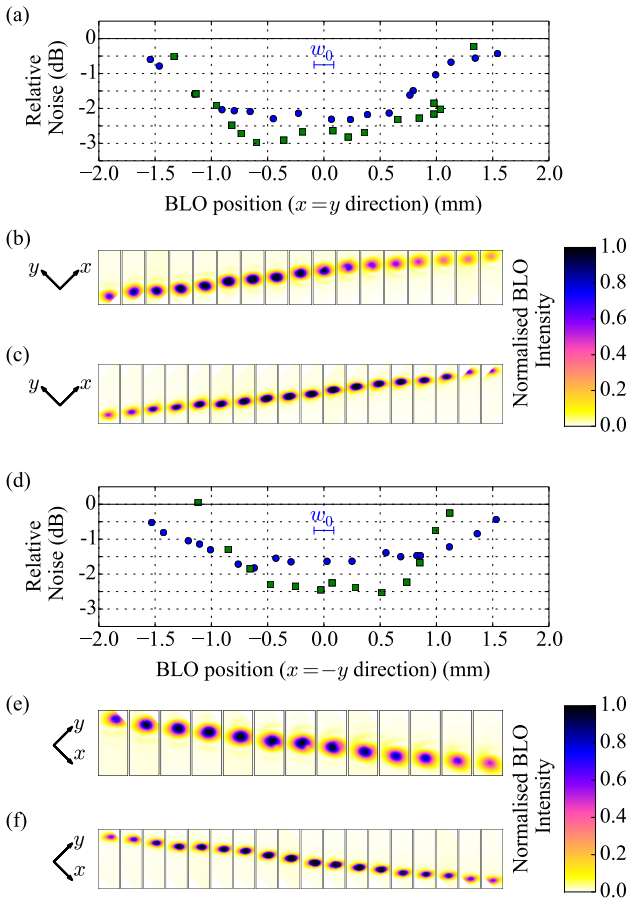

Figure 7. Local multimode squeezing. (a) Squeezing as a function of BLO position. The BLO position is extracted from (b) and (c) which show images of the BLO as it is translated along the $x = y$ direction. The series of images (b) (wider BLO) corresponds to the green squares. Series (c) (narrower BLO) corresponds to the blue circles. (d) Squeezing as a function of BLO position as it is translated along the $x = -y$ direction, again (e) and (f) show the images corresponding to the green and blue data respectively. The black lines indicate the QNL, the green squares show the data for parameters resulting in a gain of 4, with BLO mode waist dimensions of 0.45 mm by 0.61 mm, and the blue circles show the data for parameters resulting in a gain of 2, with BLO mode waist dimensions of 0.31 mm by 0.58 mm. All the results are corrected for the electronic noise floor (at −13 dB). The scale bar labelled w_0 indicates the size of the coherence area, extracted from Fig. 8

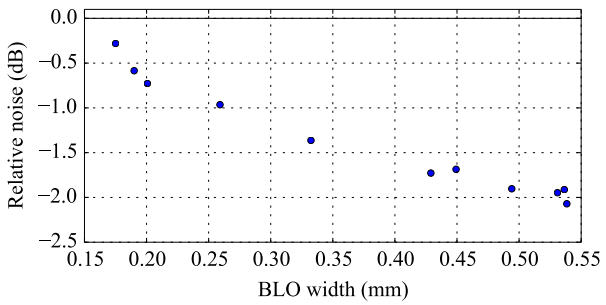

Figure 8. Quantum noise reduction as a function of the width of the BLO.

level. More generally the impact of the slit size on the squeezing level can be seen in Fig. 8. There is a small size $w_0 = 0.18$ mm of the BLO for which local squeezing can still be observed. This point is reached when the diffracted far-field size of the BLO in the same transverse direction occupies the whole RGR.

We extract from Fig. 7 the size of the squeezing region $l = 3.1$ mm in both the $x = y$ and $x = -y$ directions. Taking w_0 to be the coherence length one gets a total number of squeezed modes $l^2/4w_0^2 = 75$.

The measured coherence length can also be compared to the theoretical value of the coherence length as described by Lopez et al. [13]. It is the waist of a beam such that the Rayleigh range is equal to the length of the gain medium, and is given by

$$l_{coh} = \sqrt{\frac{\lambda l_g}{\pi n_s}}, \tag{3}$$

where n_s is the refractive index and is taken to be 1, λ is the wavelength and l_g is the length of the gain medium, in this case the rubidium cell. With the parameters in our system the theoretical coherence length is $l_{coh} = 0.056$ mm. The corresponding number of squeezed modes N is then calculated by comparing the pump waist w_p and the coherence length:

$$N = \frac{w_p^2}{l_{coh}^2}. \tag{4}$$

With our parameters this expression leads to an estimate of 300 independent modes being squeezed. However, in our experiment, we only collect and analyse a small portion of the 4WM emission annulus (see Fig. 4), and thus only have access to a fraction of these modes.

The maximum number of squeezed modes could be increased by enlarging the pump beam. Alternatively the same effect could be achieved by reducing the coherence length, which is done by reducing the length of the gain medium. Both of these adjustments would require the medium to be pumped with a higher power in order to attain the same gain.

It can be seen from Fig. 4 that the RGRs, as they are formed, have different x and y dimensions. We have checked that this results in a significant difference in the number of modes between the x and y directions.

B. Structure of the LO

It is clear from the results above that the squeezed field is spatially multimode and the BLO can have an arbitrary shape, as long as its spatial spectrum fits in the spatial bandwidth of the 4WM process. However in order to measure squeezing the probe and conjugate components of the BLO must follow the phase conjugation dictated by the 4WM. Classically, for a flat pump wavefront, this conjugation reads $E_p(\boldsymbol{\rho}) = E_c^*(\boldsymbol{\rho})$ for all $\boldsymbol{\rho}$ in the near field plane. Although this seems a rather straightforward condition to fulfil, it should be noted that not matching the BLO to the spatial structure of the squeezed vacuum leads to a rapid loss of measured squeezing [31]. Indeed squeezing measurements of multimode fields are sensitive to LO wavefront distortions. Any imperfection in the LO phase profile causes antisqueezed quadratures of higher order spatial modes to be measured alongside the squeezed quadrature of the target mode, resulting in a noise level which is typically above the QNL.

A possible solution to this experimental difficulty is to use the nonlinear process itself to create the LO bright field [25, 32]. We implement this method by stimulating the second 4WM process to generate bright probe and conjugate fields that can be used to form the BLO (Fig. 5). Provided both pumps have the same mode shape, the BLO automatically matches the structure of the squeezed vacuum, both in phase and amplitude, irrespective of the chosen pump mode and the associated phase conjugation. Note that we still need to accurately overlay the very same RGRs for both the BLO and the signal.

In spite of the strong constraints on the wavefront of the LO, it was suggested [22] that spatially multimode squeezing can improve the detection of quantum noise reduction due to the relaxed constraints on the LO shape. We could indeed verify that the measured squeezing was only mildly dependent on the overlap of the BLO with the signal in the homodyne detector (e.g. tuning of mirror M in Fig. 5).

C. Experimental limitations

There are a number of reasons why a finite amount of squeezing can be observed, well below the theoretical value dictated by the gain. The main one comes from the way the BLO is generated. Seeding at only the probe frequency induces a power imbalance between the probe and conjugate frequency components in the BLO, resulting in an uneven detection of the correlated sidebands. Increasing the gain reduces this imbalance, but increases the antisqueezing in the signal, making the squeezing measurements more sensitive to misalignment as explained

in the previous section. This trade-off sets the optimum gain value in the range of 2–4. The squeezing is also limited by other imperfections affecting the reflectance of the mirrors, the transmittance of the anti-reflection coatings and the quantum efficiency of the detectors.

Throughout this experiment we have chosen to work in the near field where the local correlations between probe and conjugate frequency components are generated. It is possible to transfer these local correlations to the far-field. Due to the theoretical axial symmetry of the correlations in the far field a flip of one of the RGRs in each of the q_x and q_y directions is required (see Fig. 4). In practice the probe and conjugate propagate differently due to the Kerr lensing of the probe in the medium, and correlated probe and conjugate modes in the far field have slightly different shapes [25]. If one is not concerned with accurate control of the LO shape, or sharply localized squeezing, then it is still possible to observe multimode squeezing in this fashion. Indeed we have successfully measured squeezing up to 2 dB in this arrangement, with results limited by the additional experimental complexity.

VI. CONCLUSION

We have demonstrated the generation of a light field which displays local squeezing in a total of 75 independent modes using a 4WM system in a hot rubidium vapour. The squeezing exists as quantum correlations between distant frequency sidebands, however our setup provides a natural way to generate the arbitrarily shaped bichromatic local oscillator required to measure the multi-spatial-mode squeezing.

Such a quantum state of light can theoretically be used to improve super-resolution techniques [9], when overlapped with a bright optical carrier to form a bright illumination. In future work, and as a step toward quantum-enhanced super-resolution, we are aiming to demonstrate local intensity quantum noise reduction of the resulting illumination in the temporal domain. Directly imaging the light with a camera in a series of snapshots should reveal local intensity fluctuations below the shot noise in arbitrary regions of the images.

This research was supported by the Engineering and Physical Sciences Research Council grants EP/E036473/1 and EP/I001743/1.

[1] Vittorio Giovannetti, Seth Lloyd, and Lorenzo Maccone, "Quantum-Enhanced Measurements: Beating the Standard Quantum Limit," Science **306**, 1330–1336 (2004).

[2] Mikhail I. Kolobov, *Quantum Imaging* (Springer, New York, 2006).

[3] G. Brida, M. Genovese, and I. Ruo Berchera, "Experimental realization of sub-shot-noise quantum imaging," Nat Photon **4**, 227–230 (2010).

[4] Takafumi Ono, Ryo Okamoto, and Shigeki Takeuchi, "An entanglement-enhanced microscope," Nat Commun **4** (2013), 10.1038/ncomms3426.

[5] Yonatan Israel, Shamir Rosen, and Yaron Silberberg, "Supersensitive Polarization Microscopy Using NOON States of Light," Phys. Rev. Lett. **112**, 103604 (2014).

[6] Lee A. Rozema, James D. Bateman, Dylan H. Mahler, Ryo Okamoto, Amir Feizpour, Alex Hayat, and Aephraim M. Steinberg, "Scalable Spatial Superresolution Using Entangled Photons," Phys. Rev. Lett. **112**, 223602 (2014).

[7] Michael A. Taylor, Jiri Janousek, Vincent Daria, Joachim Knittel, Boris Hage, Hans-A. Bachor, and Warwick P. Bowen, "Biological measurement beyond the quantum limit," Nat Photon **7**, 229–233 (2013).

[8] Michael A. Taylor, Jiri Janousek, Vincent Daria, Joachim Knittel, Boris Hage, Hans-A. Bachor, and Warwick P. Bowen, "Subdiffraction-Limited Quantum Imaging within a Living Cell," Phys. Rev. X **4**, 011017 (2014).

[9] Mikhail I. Kolobov and Claude Fabre, "Quantum Limits on Optical Resolution," Phys. Rev. Lett. **85**, 3789 (2000).

[10] Matthew Pysher, Yoshichika Miwa, Reihaneh Shahrokhshahi, Russell Bloomer, and Olivier Pfister, "Parallel Generation of Quadripartite Cluster Entanglement in the Optical Frequency Comb," Phys. Rev. Lett. **107**, 030505 (2011).

[11] Jonathan Roslund, Renn Medeiros de Arajo, Shifeng Jiang, Claude Fabre, and Nicolas Treps, "Wavelength-multiplexed quantum networks with ultrafast frequency combs," Nat Photon **8**, 109–112 (2014).

[12] M. I. Kolobov and I. V. Sokolov, "Spatial behavior of squeezed states of light and quantum noise in optical images," Sov. Phys. JETP **69**, 1097 (1989).

[13] L. Lopez, B. Chalopin, A. Rivire de la Souchre, C. Fabre, A. Matre, and N. Treps, "Multimode quantum properties of a self-imaging optical parametric oscillator: Squeezed vacuum and Einstein-Podolsky-Rosen-beams generation," Phys. Rev. A **80**, 043816 (2009).

[14] Benot Chalopin, Francesco Scazza, Claude Fabre, and Nicolas Treps, "Direct generation of a multi-transverse mode non-classical state of light," Opt. Express **19**, 4405–4410 (2011).

[15] O. Jedrkiewicz, Y.-K Jiang, E. Brambilla, A. Gatti, M. Bache, L. A. Lugiato, and P. Di Trapani, "Detection of Sub-Shot-Noise Spatial Correlation in High-Gain Parametric Down Conversion," Phys. Rev. Lett. **93**, 243601 (2004).

[16] E. Brambilla, L. Caspani, O. Jedrkiewicz, L. A. Lugiato, and A. Gatti, "High-sensitivity imaging with multi-mode twin beams," Phys. Rev. A **77**, 053807 (2008).

[17] Ivan N. Agafonov, Maria V. Chekhova, and Gerd Leuchs, "Two-color bright squeezed vacuum," Phys. Rev. A **82**, 011801 (2010).

[18] Nicolas Treps, Nicolai Grosse, Warwick P. Bowen, Claude Fabre, Hans-A. Bachor, and Ping Koy Lam, "A Quantum Laser Pointer," Science New Series, **301**, 940–943 (2003).

[19] V. Boyer, A. M. Marino, and P. D. Lett, "Generation of Spatially Broadband Twin Beams for Quantum Imaging," Phys. Rev. Lett. **100**, 143601 (2008).

[20] Neil Corzo, Alberto M. Marino, Kevin M. Jones, and Paul D. Lett, "Multi-spatial-mode single-beam quadrature squeezed states of light from four-wave mixing in hot rubidium vapor," Opt. Express **19**, 21358–21369 (2011).

[21] R. E. Slusher, L. W. Hollberg, B. Yurke, J. C. Mertz, and J. F. Valley, "Observation of Squeezed States Generated by Four-Wave Mixing in an Optical Cavity," Phys. Rev. Lett. **55**, 2409–2412 (1985).

[22] L. A. Lugiato and Ph. Grangier, "Improving quantum-noise reduction with spatially multimode squeezed light," J. Opt. Soc. Am. B **14**, 225–231 (1997).

[23] Robert W. Boyd, *Nonlinear Optics*, 3rd ed. (Academic Press, Amsterdam ; Boston, 2008).

[24] C. F. McCormick, V. Boyer, E. Arimondo, and P. D. Lett, "Strong relative intensity squeezing by four-wave mixing in rubidium vapor," Opt. Lett. **32**, 178–180 (2007).

[25] Vincent Boyer, Alberto M. Marino, Raphael C. Pooser, and Paul D. Lett, "Entangled Images from Four-Wave Mixing," Science **321**, 544 –547 (2008).

[26] N. V. Corzo, A. M. Marino, K. M. Jones, and P. D. Lett, "Noiseless Optical Amplifier Operating on Hundreds of Spatial Modes," Phys. Rev. Lett. **109**, 043602 (2012).

[27] Prem Kumar and Mikhail I. Kolobov, "Degenerate four-wave mixing as a source for spatially-broadband squeezed light," Optics Communications **104**, 374–378 (1994).

[28] M. T. Turnbull, P. G. Petrov, C. S. Embrey, A. M. Marino, and V. Boyer, "Role of the phase-matching condition in nondegenerate four-wave mixing in hot vapors for the generation of squeezed states of light," Phys. Rev. A **88**, 033845 (2013).

[29] Alberto M. Marino, Jr. Stroud, C. R., Vincent Wong, Ryan S. Bennink, and Robert W. Boyd, "Bichromatic local oscillator for detection of two-mode squeezed states of light," J. Opt. Soc. Am. B **24**, 335–339 (2007).

[30] E. Brambilla, A. Gatti, M. Bache, and L. A. Lugiato, "Simultaneous near-field and far-field spatial quantum correlations in the high-gain regime of parametric down-conversion," Phys. Rev. A **69**, 023802 (2004).

[31] Arthur La Porta and Richart E. Slusher, "Squeezing limits at high parametric gains," Phys. Rev. A **44**, 2013–2022 (1991).

[32] Chonghoon Kim and Prem Kumar, "Quadrature-Squeezed Light Detection Using a Self-Generated Matched Local Oscillator," Phys. Rev. Lett. **73**, 1605–1608 (1994).

[33] Lu-Ming Duan, G. Giedke, J. I. Cirac, and P. Zoller, "Inseparability Criterion for Continuous Variable Systems," Phys. Rev. Lett. **84**, 2722–2725 (2000).

Appendix A: Correlation propagation

Let us consider the electromagnetic field at the frequency sidebands $\pm\Omega$ propagating along the z axis. In a perpendicular plane, taken to be the near field at $z = 0$, the field operator $E(\boldsymbol{\rho}, \Omega)$ can be decomposed on the local quadrature operators, themselves expressed as local creation and annihilation operators:

$$X(\boldsymbol{\rho}, \Omega) = \frac{1}{2}\left[a^\dagger(\boldsymbol{\rho}, \Omega) + a(\boldsymbol{\rho}, \Omega)\right], \tag{A1}$$

$$Y(\boldsymbol{\rho}, \Omega) = \frac{i}{2}\left[a^\dagger(\boldsymbol{\rho}, \Omega) - a(\boldsymbol{\rho}, \Omega)\right], \tag{A2}$$

where $\boldsymbol{\rho}$ is the transverse position. The same relations hold in momentum space and equivalently, due to Fraunhofer diffraction, in the far field at $z = \infty$, the field $E(\mathbf{q}, \Omega)$ can be decomposed on:

$$X(\mathbf{q}, \Omega) = \frac{1}{2}\left[a^\dagger(\mathbf{q}, \Omega) + a(\mathbf{q}, \Omega)\right], \tag{A3}$$

$$Y(\mathbf{q}, \Omega) = \frac{i}{2}\left[a^\dagger(\mathbf{q}, \Omega) - a(\mathbf{q}, \Omega)\right], \tag{A4}$$

where $a(\mathbf{q}, \Omega)$ is the spatial Fourier transform of $a(\boldsymbol{\rho}, \Omega)$ and $a^\dagger(\mathbf{q}, \Omega)$ is the adjoint of $a(\mathbf{q}, \Omega)$. Note that $a^\dagger(\mathbf{q}, \Omega)$ is also the Fourier transform of $a^\dagger(-\boldsymbol{\rho}, \Omega)$. In effect, this means that $X(\mathbf{q}, \Omega)$ is not the Fourier transform of $X(\boldsymbol{\rho}, \Omega)$. Physically, this property reflects the phase-matching condition and as we will now see, it transforms local correlations in the near field into symmetric correlations between $\mathbf{q}$ and $-\mathbf{q}$ in the far field.

A thin nonlinear medium at $z = 0$, where propagation and the associated diffraction can be neglected, creates local correlations which depend on the local phase of the pump field. For instance for a pump with a infinite flat wavefront (i.e. with a well defined wavevector $\mathbf{k}_0$), the following two joint quadratures are squeezed for all $\boldsymbol{\rho}$:

$$X_-(\boldsymbol{\rho}, \Omega) = \frac{1}{\sqrt{2}}\left[X(\boldsymbol{\rho}, \Omega) - X(\boldsymbol{\rho}, -\Omega)\right], \tag{A5}$$

$$Y_+(\boldsymbol{\rho}, \Omega) = \frac{1}{\sqrt{2}}\left[Y(\boldsymbol{\rho}, \Omega) + Y(\boldsymbol{\rho}, -\Omega)\right]. \tag{A6}$$

In the far field, one can form another joint quadrature and express it as a function of $X_-(\boldsymbol{\rho}, \Omega)$ and $Y_+(\boldsymbol{\rho}, \Omega)$:

$$\begin{aligned} X_-(\mathbf{q}, \Omega) &= \frac{1}{\sqrt{2}}\left[X(\mathbf{q}, \Omega) - X(-\mathbf{q}, -\Omega)\right] \\ &= \frac{1}{2\sqrt{2}}\left[a^\dagger(\mathbf{q}, \Omega) + a(\mathbf{q}, \Omega)\right. \\ &\quad \left. - a^\dagger(-\mathbf{q}, -\Omega) - a(-\mathbf{q}, -\Omega)\right] \\ &= \frac{1}{2\sqrt{2}}\mathcal{F}\left[a^\dagger(-\boldsymbol{\rho}, \Omega)\right. \\ &\quad \left. + a(\boldsymbol{\rho}, \Omega) - a^\dagger(\boldsymbol{\rho}, -\Omega) - a(-\boldsymbol{\rho}, -\Omega)\right] \\ &= \frac{1}{\sqrt{2}}\mathcal{F}\left[X_-(\boldsymbol{\rho}, \Omega) + X_-(-\boldsymbol{\rho}, \Omega)\right], \end{aligned} \tag{A7}$$

where $\mathcal{F}$ is the Fourier transform operation. Since $X_-(\boldsymbol{\rho}, \Omega)$ is squeezed for all $\boldsymbol{\rho}$ then so is $X_-(\mathbf{q}, \Omega)$ for

all $\mathbf{q}$. In a similar fashion, one can show that the same result applies to

$$Y_+(\mathbf{q},\Omega) = \frac{1}{\sqrt{2}}\left[Y(\mathbf{q},\Omega) + Y(-\mathbf{q},-\Omega)\right]. \quad \text{(A8)}$$

This implies that the fields at positions $\pm\mathbf{q}$ are entangled [33]. Ref. 30 gives an account of the near- and far-field correlations for the intensity.

We now show that the overlapping operation shown in Fig. 4 preserves the local correlations in the near field while restricting the accessible spatial spectrum of the fluctuations to the positive side. By overlapping two opposite RGRs of the emission annulus in the far field, one translates the fields transversely by $\pm\mathbf{q}_0$. As a result, the creation operator transforms as:

$$a'(\mathbf{q},\Omega) = \frac{1}{\sqrt{2}}[a(\mathbf{q}-\mathbf{q}_0,\Omega) + a(\mathbf{q}+\mathbf{q}_0,\Omega)], \quad \text{(A9)}$$

with $q_x \in [-q_0, q_0]$. The phase of the superposition is arbitrary and has no bearing on the final conclusion. According to Eqs. (A8) and (A7), the entanglement occurs between opposite sidebands $\pm\Omega$ and opposite transverse wavevectors $\pm\mathbf{q}$. For now, we restrict ourselves to a particular pair of correlated sidebands, where the Ω sideband comes from the left RGR and the $-\Omega$ sideband comes from the right RGR. Within this simplification, the creation operator is:

$$a'(\mathbf{q},\pm\Omega) = a(\mathbf{q}\pm\mathbf{q}_0,\pm\Omega) \quad \text{(A10)}$$

or equivalently, in the near field:

$$a'(\boldsymbol{\rho},\pm\Omega) = a(\boldsymbol{\rho},\pm\Omega)e^{\mp i\varphi}, \quad \text{(A11)}$$

with $\varphi = \mathbf{q}_0\cdot\boldsymbol{\rho}$. From this we can derive the quadrature transformations:

$$X'(\boldsymbol{\rho},\pm\Omega) = X(\boldsymbol{\rho},\pm\Omega)\cos\varphi + Y(\boldsymbol{\rho},\pm\Omega)\sin\varphi, \quad \text{(A12)}$$
$$Y'(\boldsymbol{\rho},\pm\Omega) = Y(\boldsymbol{\rho},\pm\Omega)\cos\varphi - X(\boldsymbol{\rho},\pm\Omega)\sin\varphi, \quad \text{(A13)}$$

and directly we get:

$$X'_-(\boldsymbol{\rho},\Omega) = X_-(\boldsymbol{\rho},\Omega)\cos\varphi - Y_+(\boldsymbol{\rho},\Omega)\sin\varphi, \quad \text{(A14)}$$
$$Y'_+(\boldsymbol{\rho},\Omega) = X_-(\boldsymbol{\rho},\Omega)\sin\varphi + Y_+(\boldsymbol{\rho},\Omega)\cos\varphi. \quad \text{(A15)}$$

Since the joint quadratures $X_-(\boldsymbol{\rho},\Omega)$ and $Y_+(\boldsymbol{\rho},\Omega)$ are locally squeezed, this is also the case for the output joint quadratures $X'_-(\boldsymbol{\rho},\Omega)$ and $Y'_+(\boldsymbol{\rho},\Omega)$. The output field also has a contribution from the other possible configuration, where the Ω sideband comes from the right RGR and the $-\Omega$ sideband comes from the left RGR. This contribution has output joint quadratures that are similar to those given in Eqs. (A14) and (A15). Both contributions are uncorrelated and their noises add in quadrature, so that their superposition is also squeezed. As a result the output field displays the same local squeezing as the field inside the nonlinear medium, while having a continuous spatial spectrum centered on 0 for both the x and y directions.

We have considered here a medium of zero length, which results in perfectly localized squeezing. In practice the cell has a finite length, which gives rise to a finite minimum size of a squeezed area, called coherence length. This is studied in section V-A.

Appendix B: Experimental details

To ensure relative phase stability, all laser beams are derived from a single a Titanium:Sapphire laser, tuned approximately 800 MHz from the $5^2S_{1/2}\,(F=2) \rightarrow 5^2P_{1/2}$ atomic transition at 795 nm. The main laser beam is split, with two equal parts being used for the LO pump and the signal pump at 900 mW, and a final small portion being used to generate the seed beam at the probe frequency. To do this an acousto-optic modulator (AOM) is operated at 1.520 GHz in a double pass arrangement. The seed beam has a power of 130 μW. It is amplified by the 4WM, with a gain of around 4 with our parameters, and is used to generate a BLO with a total power of up to 910 μW. The pump beam has a waist of 1 mm in the centre of the cell, whilst the unvignetted seed beam has a waist of 0.35 mm. All of the noise signals are measured with a spectrum analyser using a detection frequency of 1 MHz, a resolution bandwidth of 100 kHz and video bandwidth of 30 Hz. To obtain the largest possible squeezing spatial bandwidth the parameters are tweaked such that the BLO pump power is 1.3 W, the signal pump power is 580 mW, and the AOM is operated at 1.523 GHz. This leads to a gain of around 2, and a final BLO power of 215 μW.

A 12.5 mm-long rubidium vapour cell, heated to $\approx$ 120°C, forms the gain medium. The cell is contained within a vacuum chamber to avoid the convection air currents around the heat pipe, and hence eliminate wavefront distortions due to refractive index fluctuations on the signal and BLO optical paths.

The production of quadrature squeezing on the overlapping beamsplitter occurs only when the phase difference between the two RGRs at the beamsplitter is the same for both the probe and the conjugate. We ensure this condition by adjusting the difference in the optical path of the two RGRs from the cell to the overlapping beamsplitter to an inaccuracy much smaller than the beat length between the probe and the conjugate (5 cm, corresponding to a frequency difference of $\omega_c - \omega_p =$ 6 GHz). To achieve this we temporarily seed the signal 4WM process symmetrically with one seed in each RGR, and use the visibility of the resulting bichromatic interference on the overlapping beamsplitter to minimise the path length difference. Typically a visibility of 99% can be achieved. Similarly to ensure a good overlap between the two frequency components of the LO we use independent interferences between each of the components of the LO and the corresponding component of the previously aligned seeded signal modes.

To control the size of the BLO in the direction of in-

terest we clip the seed with a slit made up of two razor blades. The sharp edges of the slit introduce high-order spatial modes, with large $|\mathbf{q}|$, lying outside of the spatial gain profile. These high-order modes will only be present in the probe frequency component. A filtering iris is placed in the Fourier plane to remove these spatial frequencies before the 4WM cell. The iris size is adjusted to cut at the first zero in the Fourier spectrum.

In order to be able to measure the squeezing using the homodyne detection and also image the BLO modes on a camera, a flip mirror is used to control the direction of the beam incident on one side of the balanced detector. A single lens images the near-field gain region on the camera.